Tunable enhancement of exciton emission from MgZnO by hybridized quadrupole plasmons in Ag nanoparticle aggregation

Hong-Yu Chen,[1,2] Ke-Wei Liu,[1,a)] Ming-Ming Jiang,[1] Zhen-Zhong Zhang,[1] Xiu-Hua Xie,[1,2] Deng-Kui Wang,[1,2] Lei Liu,[1] Bing-Hui Li,[1] Dong-Xu Zhao,[1] Chong-Xin Shan,[1] and De-Zhen Shen[1,b)]

[1]*State Key Laboratory of Luminescence and Applications, Changchun Institute of Optics, Fine Mechanics, and Physics, Chinese Academy of Sciences, Changchun 130033, People Republic of China*

[2]*Graduate University of the Chinese Academy of Sciences, Beijing 100049, People Republic of China*

(Received 16 January 2014; accepted 22 February 2014; published online 5 March 2014)

$Mg_{0.2}Zn_{0.8}O$/metal nanoparticle systems have been fabricated and investigated. The photoluminescence results indicate that Al and Au nanoparticles could slightly enhance the near-band-edge (NBE) emission from $Mg_{0.2}Zn_{0.8}O$. In contrast, a giant and tunable NBE emission enhancement could be induced by Ag nanoparticles based on the coupling interaction between the hybridized quadrupole plasmon in Ag nanoparticle aggregation and the excitons of $Mg_{0.2}Zn_{0.8}O$. Interestingly, the intensity and position of the narrow quadrupole resonance could be controlled by tuning the interspace gap and size of Ag nanoparticles, which was clearly demonstrated both experimentally and theoretically. Our findings may pave the way for further development of high-efficiency UV light-emitting devices. © *2014 AIP Publishing LLC*. [http://dx.doi.org/10.1063/1.4867777]

ZnO and its ternary alloy MgZnO have received much attention due to their potential applications in the short-wavelength optoelectronic devices such as light-emitting diodes (LEDs) and laser diodes.[1–4] Till now, various ZnO-based light-emitting devices have been reported, but their UV emission intensity is still very weak due to lack of high quality p-type ZnO (MgZnO). To overcome this problem, most of the studies focused on how to improve the quality of p-ZnO.[5,6] However, the fabrication of high quality p-ZnO is still a big challenge. Thus, before the breakthrough in p-type doping of ZnO based materials, achieving a highly effective improvement in the UV emission intensity of existing devices is a more feasible method from the practical point of view. In the previous reports, surface plasmons (SPs) have been widely used to improve the emission efficiency of light-emitting materials and devices.[7–13] SPs-induced emission enhancements are usually based on the dipole resonance, which is the most easily realized mode among the surface plasmon resonance modes. However, most metals have plasmonic dipole resonances at visible or IR range, and it is difficult to realize an effective UV emission enhancement due to a large energy separation. Additionally, owing to the broadband feature of dipole plasmon modes, the conventional emission enhancements always show weak wavelength controllable, and some undesired enhancement is usually generated at the same time. In our previous report, a narrow-band hybridized quadrupole resonance has been demonstrated in the UV range in random Ag nanoclusters.[14,15] Thus, a highly controllable enhancement of UV emission is expected to be realized by the narrow quadrupole modes.

In this letter, we report a giant UV emission enhancement from $Mg_{0.2}Zn_{0.8}O$ induced by the random Ag nanoparticles (NPs). More interestingly, this UV emission enhancement is highly dependent on the wavelength, which is determined by the frequency of the narrow quadrupole modes of Ag NPs. The extinction and photoluminescence (PL) spectra were measured to investigate the coupling between the quadrupole plasmons and excitons. The finite difference time-domain (FDTD) simulations illustrated the origin and shift of the Ag hybridized quadrupole resonance.

Ag, Al, and Au (99.99%) were evaporated onto the sapphire under a pressure of about 2×10^{-3} Pa using a evaporated technique at room temperature, subsequently, annealed at 450 °C to form metal nanostructures, N_2 was used to prevent oxidation of the metal nanostructures during annealing. Then, ~300 nm hexagonal $Mg_{0.2}Zn_{0.8}O$ epilayers were deposited directly on c-plane (0001) sapphire substrate with and without metal nanostructures by metal organic chemical vapor deposition (MOCVD) at 450 °C, with the pressure of 2×10^4 Pa. Highly pure Oxygen (99.999%), diethylzinc (DEZn), and dimethyl dicyclopentadienyl magnesium ($(MeCp)_2Mg$) were employed as the precursors and highly pure nitrogen (99.999%) was used as the carrier gas.

The morphology of the metal nanostructures and the thickness of MgZnO films were characterized by a Hitachi S4800 field-emission scanning electron microscope (FESEM). Energy-dispersive X-ray spectroscopy (EDS) was used to determine the composition of the MgZnO films, and their crystal structure was studied using a Bruker D8 X-ray diffractometer. PL signals of the samples were collected using a SPEX 1404 monochromator with a continuous-wave He-Cd laser (325 nm) as the excitation source with the excitation density of 70 W/cm^2. The extinction spectra measurement were carried out by a Shimadzu UV-3101PC scanning spectrophotometer.

Fig. 1(a) shows the schematic structures of MgZnO/sapphire and MgZnO/metal/sapphire. All the samples have almost the same MgZnO layer with the thickness of ~300 nm, which allows us to compare the PL efficiency purely induced by the metal nanostructures. The EDS result

a)Electronic mail: Liukw@ciomp.ac.cn
b)Electronic mail: Shendz@ciomp.ac.cn

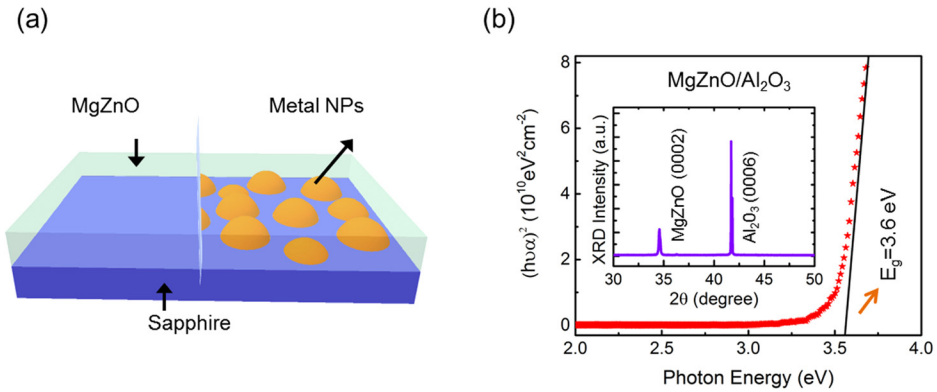

FIG. 1. (a) Schematic structures of $Mg_{0.2}Zn_{0.8}O$/sapphire and $Mg_{0.2}Zn_{0.8}O$/metal/sapphire. (b) $(\alpha h\nu)^2$ as a function of energy ($h\nu$) based on the experimental absorption spectrum of bare $Mg_{0.2}Zn_{0.8}O$, and the inset is the XRD pattern of $Mg_{0.2}Zn_{0.8}O$ film.

indicated that the composition of MgZnO alloy films is $Mg_{0.2}Zn_{0.8}O$. Fig. 1(b) shows the relationship of $(\alpha h\nu)^2$ (where α is the absorption coefficient; h is the Planck constant) as a function of energy ($h\nu$). The band gap energy of $Mg_{0.2}Zn_{0.8}O$ alloy was determined to be ~3.6 eV from an obtained UV-visible absorption spectrum. The x-ray diffraction (XRD) result indicates that the $Mg_{0.2}Zn_{0.8}O$ films have hexagonal wurtzite structure with c-axis preferred orientation as shown in the inset of Fig. 1(b).

In order to investigate the effect of different metals on the optical property of $Mg_{0.2}Zn_{0.8}O$ film, the room-temperature PL spectra of bare $Mg_{0.2}Zn_{0.8}O$, $Mg_{0.2}Zn_{0.8}O$/Ag, $Mg_{0.2}Zn_{0.8}O$/Al, and $Mg_{0.2}Zn_{0.8}O$/Au are shown in Fig. 2(a). The UV emission was photoexcited and measured from the top of $Mg_{0.2}Zn_{0.8}O$ films with and without metals. For the bare $Mg_{0.2}Zn_{0.8}O$, a weak near-band-edge (NBE) emission can be observed around 350 nm. Interestingly, the hybrid samples showed an obvious NBE emission enhancement induced by the metal nanostructures. The inset of Fig. 2(a) compares the integrated PL enhancement ratio by Ag, Al, and Au nanostructures. It can be found that the NBE emission from

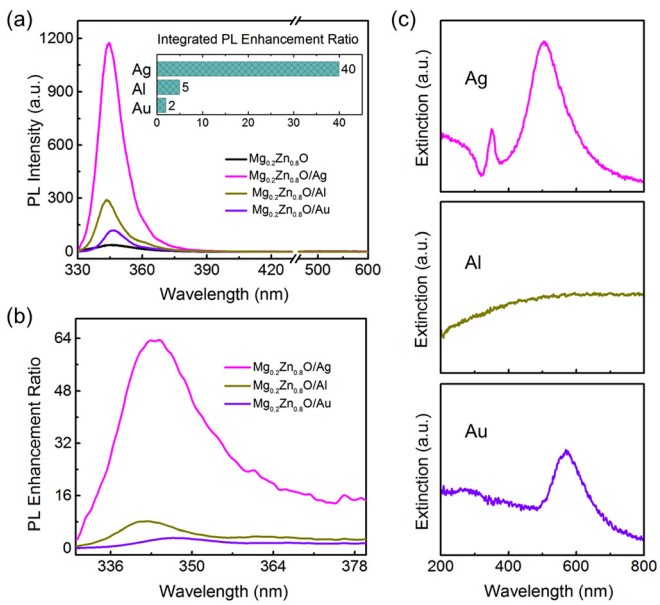

FIG. 2. (a) the PL spectra of bare $Mg_{0.2}Zn_{0.8}O$, $Mg_{0.2}Zn_{0.8}O$/Ag, $Mg_{0.2}Zn_{0.8}O$/Al, and $Mg_{0.2}Zn_{0.8}O$/Au. The inset is the integrated PL enhancement ratio of different samples; (b) the PL enhancement ratio as a function of the wavelength. (c) Extinction spectra of Ag, Al, and Au nanoparticles.

$Mg_{0.2}Zn_{0.8}O$ was enhanced 40-fold, 5-fold, and 2-fold in $Mg_{0.2}Zn_{0.8}O$/Ag, $Mg_{0.2}Zn_{0.8}O$/Al, and $Mg_{0.2}Zn_{0.8}O$/Au samples, respectively. To better understand the SPs-enhanced NBE emission, the enhancement ratios of PL intensity as a function of the wavelength are shown in Fig. 2(b). We find that the enhancement ratios in the UV range for Ag sample are very large and they are strongly dependent on the wavelength. As for Al and Au samples, their enhancement ratios are relatively small with weak wavelength dependence. The giant PL enhancement of Ag sample may be derived from the strong SPs-excitons interaction.

As is well known, a good energy match between the light emission and SPs is the key factor to achieve giant SPs-induced emission enhancement. To get insight in the difference of NBE emission enhancements, the extinction spectra of Ag, Al, and Au nanostructures were shown in Fig. 2(c). For Ag nanostructures, two extinction peaks can be clearly observed. According to our previous work, the extinction peaks located at visible and UV ranges of Ag nanostructures should be assigned to the hybridized dipole and quadrupole modes, respectively.[14,15] Notably, the peak of hybridized quadrupole modes in the UV range is very narrow. In contrast, only one extinction peak located at visible range can be observed for Au sample, whereas there is no obvious peak for Al sample. It is worth mentioning here that all the metal nanostructures which have the similar morphology were fabricated by the same process. Based on the analysis of the extinction spectra, in Fig. 2(c) and the PL results in Figs. 2(a) and 2(b), we think that the giant PL enhancement of Ag sample was mainly attributed to the strong quadrupoles-excitons interaction. As for Al and Au samples, their weak enhancements could be explained by the charge transition between the metal and the semiconductor and the scattering effect of the metal NPs.[8,10,11,13] Therefore, it can be concluded that Ag nanostructure is the most promising candidate for the highly controllable enhancement of UV emission due to their narrow quadrupole plasmon resonance in the UV range. And this conclusion is corresponding well with the PL spectra in Fig. 2(a).

To further investigate the tunable enhancement of NBE excitons from $Mg_{0.2}Zn_{0.8}O$ alloys by quadrupole of Ag nanostructures, Ag thin films with various thicknesses were evaporated on the sapphire substrate and then annealed to form Ag nanostructures with different morphologies. As is shown in the right panel of Fig. 3(a), Ag nanostructures are globoid or ellipsoid in shape and randomly dispersed onto the sapphire

with the average diameter of ~60, ~80, and ~100 nm, which are labeled as Ag (S1), Ag (S2), and Ag (S3), respectively. The left panel of Fig. 3(a) shows the extinction spectra of Ag (S1), Ag (S2), and Ag (S3). With increasing the average diameter of Ag NPs, the broad dipole resonance peak is significantly red-shifted in the visible regime. In contrast, the quadrupole mode with a narrow linewidth (shaded region) could be tailored more minutely in the UV range, which will be benefit for the highly tunable enhancement of exciton emission from $Mg_{0.2}Zn_{0.8}O$. Fig. 3(b) shows the PL spectra of bare $Mg_{0.2}Zn_{0.8}O$ and $Mg_{0.2}Zn_{0.8}O$/Ag at room temperature, and the inset compares the integrated PL enhancement ratios of $Mg_{0.2}Zn_{0.8}O$/Ag (S1), $Mg_{0.2}Zn_{0.8}O$/Ag (S2), and $Mg_{0.2}Zn_{0.8}O$/Ag (S3). It can be found that the NBE emission was enhanced 37-fold, 19-fold, and 10-fold for $Mg_{0.2}Zn_{0.8}O$/Ag (S1), $Mg_{0.2}Zn_{0.8}O$ (S2), and $Mg_{0.2}Zn_{0.8}O$/Ag (S3), respectively. Ag (S1), Ag (S2), and Ag (S3) have the similar intensity of quadrupole resonance as shown in Fig. 3(a), By comparing the PL spectra in Fig. 3(b) to the extinction spectra in Fig. 3(a), we can find that the peak shift of NBE emission from $Mg_{0.2}Zn_{0.8}O$ shows a similar trend with that of the hybridized quadrupole resonance with increasing the size of Ag NPs. Thus, the difference in their integrated PL enhancement ratios should associate with the energy matching between the excitons of $Mg_{0.2}Zn_{0.8}O$ and the quadrupole resonance of Ag. Fig. 3(c) shows the PL enhancement ratios as a function of the wavelength for the hybrid samples, and it can be found that the maxima of the PL enhancement ratios are red-shifted with the increase in the size of Ag nanoparticles, which is in good agreement with the shift of the quadrupole resonance peaks. Interestingly, a clear peak can be observed at ~356 nm for all hybrid samples in the PL enhancement spectra, independent of the size of Ag NPs. Thus, this peak may be associated with the high density excitons such as localized excitons. Additionally, comparing with the previous reports, the PL enhancement spectra have very narrow line widths, indicating the excellent wavelength selectivity.[7,13]

As is aforementioned, the tunable UV light enhancement via the plasmons-excitons coupling was highly dependent on the frequency of hybridized quadrupole resonance. To shed light on the origin and the shift of the hybridized quadrupole resonance in the Ag NPs, FDTD simulations were carried out. As is well known, the spectral shape and position of the SPs resonances in the metal nanoparticle aggregation are highly sensitive to their size, shape, and internal gap.[16–19] Fig. 4 shows the calculated extinction spectra based on the optical constants measured by Johnson and Christy.[20] In Fig. 4(a), besides the dipole modes, the quadrupole resonance peak can be clearly observed in the single sphere with the diameter larger than 60 nm. With increasing the size of sphere, the quadrupole resonance intensity becomes stronger. These results indicate that the high order SPs modes could occur in the isolated NPs with relatively large size due to the inhomogeneous distribution of electron density.[19] In addition, with increasing the sphere size, the dipole peak was significantly red-shifted, while the quadrupole peak only showed a tiny red shift. In Fig. 4(b), the similar phenomenon can be observed for the single ellipsoid. Although the quadrupole modes could appear both in single spherical and non-spherical NPs, their intensity is too weak.

According to the previous reports, the interparticles interaction could lead to the change in the intensity and the location of plasmon resonance.[16–18] Considering the random dispersion of Ag NPs in our experiment, the interaction among the NPs should strongly affect the plasmon resonance, which is sensitive to the size of the NPs and their interspace gap. Figs. 4(c) and 4(d) showed the calculated extinction spectra of the hetero-dimer NPs as a function of the size and the interspace gap, respectively. In Fig. 4(c), the extinction spectra of the dimer with a nano-sphere (diameter d = 70 nm) and a nano-ellipsoid (long axis a = 70-140 nm and short axis b = 60 nm) were shown and the interspace gap (g) between two NPs is 10 nm. It can be found that the quadrupole intensity is stronger than that of the single nano-ellipsoid or nano-sphere with the same size in Figs. 4(a) and 4(b). In addition, with the increase in a of the nano-ellipsoid in dimer, the dipole and quadrupole resonances become stronger and their peaks shift to longer wavelengths. To

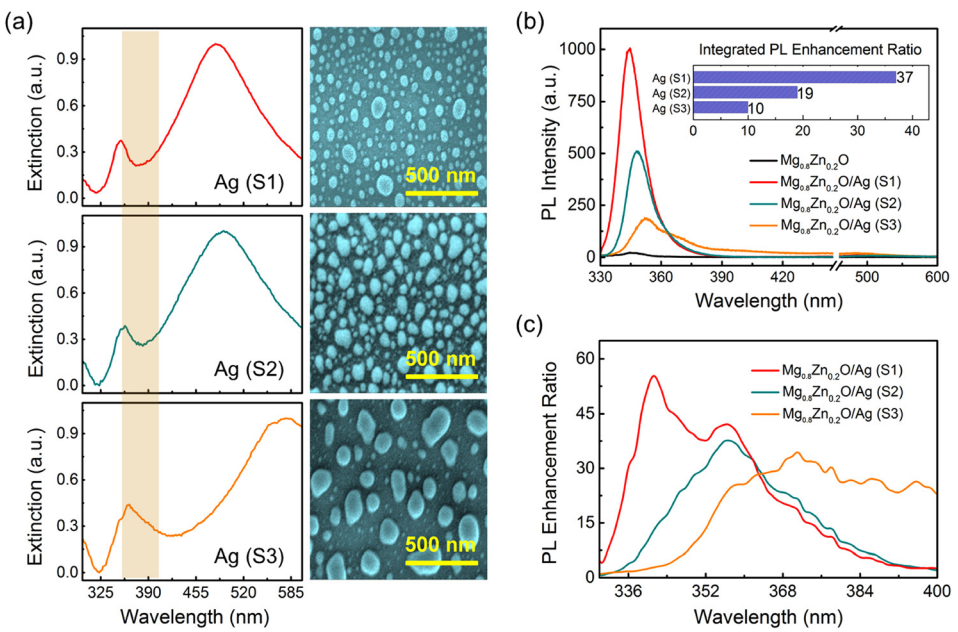

FIG. 3. (a) Extinction spectra of Ag(S1), Ag(S2), and Ag(S3). The corresponding SEM images are shown in the right panel. (b) The PL intensity of bare $Mg_{0.2}Zn_{0.8}O$, $Mg_{0.2}Zn_{0.8}O$/Ag (S1), $Mg_{0.2}Zn_{0.8}O$/Ag (S2), and $Mg_{0.2}Zn_{0.8}O$/Ag (S3). The inset is the integrated PL integrated enhancement ratio of different samples. (d) The PL enhancement ratio as a function of the wavelength.

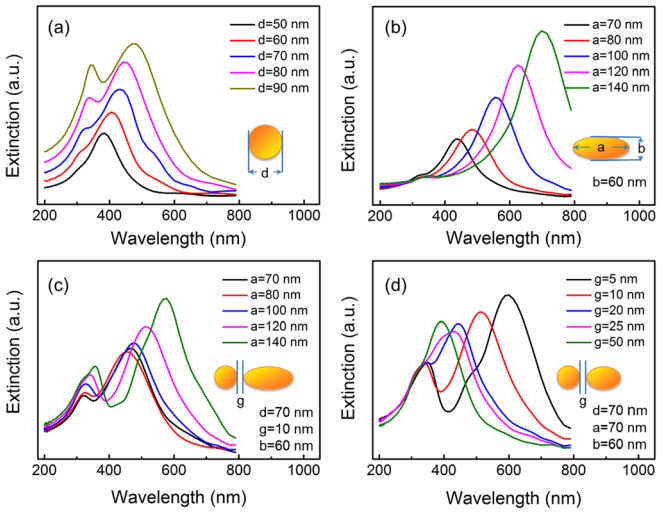

FIG. 4. Extinction spectra calculated by FDTD simulation at the wavelength of 350 nm for different conditions: (a) single nano-sphere with the diameter d ranging from 50 nm to 90 nm; (b) single nano-ellipsoid with the long axis of 70–140 nm and the short axis of 60 nm; (c) hetero-dimer consists of a nano-sphere and a nano-ellipsoid with the interspace gap of 10 nm. The diameter of nano-sphere is fixed at 70 nm, and the nano-ellipsoid has the long axis a of 70–140 nm and the short axis b of 60 nm; (d) hetero-dimer consists of a nano-sphere (d = 70 nm) and a nano-ellipsoid (a = 70 nm and b = 60 nm) with the interspace gap of 5–50 nm.

further illustrate the coupling interaction among the Ag aggregation, the calculated extinction spectra of the hetero-dimer NPs (nano-sphere: d = 70 nm; nano-ellipsoid: a = 70 nm and b = 60 nm) with various interspace gaps (g = 5–50 nm) are shown in Fig. 4(d). With decreasing g, the quadrupole resonance intensity increases and the Fano-like dip became deep obviously. This trend is mainly derived from the increase in the coupling strength with decreasing g. Meanwhile, the frequency of the quadrupole shows almost no change with the decrease in g, while the dipole plasmon resonance red shifts.

In our experiment, the random Ag NPs can be qualitatively recognized as the collection of the dimers, although we cannot completely exclude the contribution of the interaction between the dimers. The experiment results in Fig. 2(a) can be well explained by the simulation results. With increasing the average size of the random Ag NPs, the dipole peak was significantly red-shifted, while the quadrupole peak only showed a tiny red shift. In addition, the quadrupole resonances intensity in the Ag nanoparticle aggregation could be controlled by tuning the density of NPs. The manipulation of the quadrupole resonance allows us to investigate the tunable enhancement of UV emission. Based on the theoretical calculation and experimental results, it can be concluded that the quadrupole SPs in Ag nanoparticle aggregation can be actively controlled by tuning the morphology and density of Ag NPs, which could in turn enhance the NBE exciton emission from $Mg_{0.2}Zn_{0.8}O$ in UV range.

In summary, highly tunable enhancement of NBE emission from $Mg_{0.2}Zn_{0.8}O$ has been realized by the quadrupole plasmon resonance in Ag nanoparticle aggregation. The intensity and peak position of quadrupole resonance can be controlled by turning the size and density of Ag NPs. The NBE UV emission enhancement of $Mg_{0.2}Zn_{0.8}O$ was very sensitive to the frequency of the quadrupole resonance, and the room temperature enhancement ratio could reach as high as 40-fold. In contrast, only a very weak UV enhancement can be observed for Al and Au samples, which could be explained by the charge transition between the metal and the semiconductor and the scattering effect of the metal NPs. Our result gives a fundamental new insight into the highly tunable enhancement of the UV emission through the NBE excitons-quadrupole plasmons coupling. In addition, the ability to control the interaction between nanoscale plasmons and excitons would open up a wealth of possible applications for ZnO-based as well as other UV light-emitting devices with high emission efficiency.

This work was supported by the National Basic Research Program of China (973 program) (Nos. 2011CB302006, 2011CB302004, and 2011CB302002), the National Natural Science Foundation of China (Nos. 10974197, 11174273, 11104265, and 21101146), the 100 Talents Program of the Chinese Academy of Sciences.

[1]A. Tsukazaki, A. Ohtomo, T. Onuma, M. Ohtani, T. Makino, M. Sumiya, K. Ohtani, S. F. Chichibu, S. Fuke, Y. Segawa *et al.*, Nature Mater. **4**, 42–46 (2005).
[2]Z. Tang, G. K. Wong, P. Yu, M. Kawasaki, A. Ohtomo, H. Koinuma, and Y. Segawa, Appl. Phys. Lett. **72**, 3270–3272 (1998).
[3]J.-H. Lim, C.-K. Kang, K.-K. Kim, I.-K. Park, D.-K. Hwang, and S.-J. Park, Adv. Mater. **18**, 2720–2724 (2006).
[4]Ü. Özgür, Y. I. Alivov, C. Liu, A. Teke, M. Reshchikov, S. Doğan, V. Avrutin, S.-J. Cho, and H. Morkoc, J. Appl. Phys. **98**, 041301 (2005).
[5]L. Liu, J. Xu, D. Wang, M. Jiang, S. Wang, B. Li, Z. Zhang, D. Zhao, C.-X. Shan, B. Yao *et al.*, Phys. Rev. Lett. **108**, 215501 (2012).
[6]K.-K. Kim, H.-S. Kim, D.-K. Hwang, J.-H. Lim, and S.-J. Park, Appl. Phys. Lett. **83**, 63–65 (2003).
[7]K. Okamoto, I. Niki, A. Shvartser, Y. Narukawa, T. Mukai, and A. Scherer, Nature Mater. **3**, 601–605 (2004).
[8]C. W. Cheng, E. J. Sie, B. Liu, C. H. A. Huan, T. C. Sum, H. D. Sun, and H. J. Fan, Appl. Phys. Lett. **96**, 071107 (2010).
[9]K. Liu, Y. Tang, C. Cong, T. C. Sum, A. C. H. Huan, Z. Shen, L. Wang, F. Jiang, X. W. Sun, and H. Sun, Appl. Phys. Lett. **94**, 151102 (2009).
[10]M. Liu, R. Chen, G. Adamo, K. F. MacDonald, E. J. Sie, T. C. Sum, N. I. Zheludev, H. D. Sun, and H. J. Fan, Nanophotonics **2**, 153–160 (2013).
[11]B. J. Lawrie, R. Mu, and R. F. Haglund, Proc. SPIE **7394**, 73941V (2009).
[12]G. Lozano, D. J. Louwers, S. R. Rodríguez, S. Murai, O. T. Jansen, M. A. Verschuuren, and J. G. Rivas, Light: Sci. Appl. **2**, e66 (2013).
[13]B. J. Lawrie, R. F. Haglund, Jr., and R. Mu, Opt. Express **17**, 2565–2572 (2009).
[14]M.-M. Jiang, H.-Y. Chen, B.-H. Li, K.-W. Liu, C.-X. Shan, and D.-Z. Shen, J. Mater. Chem. C **2**, 56–63 (2014).
[15]H.-Y. Chen, K.-W. Liu, M.-M. Jiang, Z.-Z. Zhang, L. Liu, B.-H. Li, X.-H. Xie, F. Wang, D.-X. Zhao, C.-X. Shan *et al.*, J. Phys. Chem. C **118**, 679–684 (2014).
[16]Z. J. Yang, Z. S. Zhang, L. H. Zhang *et al.*, Opt. Lett. **36**, 1542–1544 (2011).
[17]E. Prodan, C. Radlok, N. Halas, and P. Nordlander, Science **302**, 419–422 (2003).
[18]J. Ye, F. Wen, H. Sobhani, J. B. Lassiter, P. V. Dorpe, P. Nordlander, and N. J. Halas, Nano Lett. **12**, 1660–1667 (2012).
[19]C. Noguez, J. Phys. Chem. C **111**, 3806–3819 (2007).
[20]P. B. Johnson and R.-W. Christy, Phys. Rev. B **6**, 4370 (1972).